

THE DEPTH OF THE OCTOBER 1981 OFF CHILE OUTER-RISE EARTHQUAKE ($M_s = 7.2$) ESTIMATED BY A COMPARISON OF SEVERAL WAVEFORM INVERSION METHODS

BY SATORU HONDA,* HITOSHI KAWAKATSU, AND TETSUZO SENO†

ABSTRACT

The determination of source depth of the October 1981 ($M_s = 7.2$) outer-rise earthquake off the Chilean coast has important implications for the stress state of the subducting plate. We analyze the Chile earthquake using three different waveform inversion methods in order to check the consistency of these methods and to estimate the source depth. The methods we used are:

- (1) Honda and Seno's (1989) inversion method in which we incorporate both long-period P waves and surface waves.
- (2) Nábělek's (1984) body-wave inversion methods for long-period P and SH waves.
- (3) Seno and Honda's (1988) deconvolution method in which we assume vertically distributed point sources and use long-period P waves.

These methods give consistent results which suggest that the centroid depth and depth extent of the Chile earthquake lies between 20 to 45 km, measured from the sea surface. This conclusion is contradictory to those obtained by the previous workers who prefer a shallow (<25 km) source depth. We found that the GDSN long-period data alone cannot constrain the source depth well. The shape of deconvolved source-time function is found to be strongly dependent on the assumption of point and distributed sources and the crustal structure used in the deconvolution. The source depth obtained in this study shows that the 1981 Chile outer-rise earthquake possibly occurred because of the compression associated with the bending of the subducting plate.

INTRODUCTION

The October 1981 Chile earthquake (hereafter identified by CE) occurred near the outer-rise area (Fig. 1) and is considered to be an important indicator of the stress state of subducting lithosphere. Usually, those earthquakes which occur in the outer-rise area are interpreted as "bending earthquakes" (Stauder, 1968; Chapple and Forsyth, 1979). Chapple and Forsyth (1979) compiled bending earthquakes and found that they are basically classified into two groups; either the extensional or compressional principal axis is horizontal and almost perpendicular to the trench axes. The source depths of the extension type earthquakes were found to be shallower than those of the compression type earthquakes. From these results, Chapple and Forsyth (1979) concluded that the origin of the stress which generates those events is a bending of lithosphere before subduction.

The focal mechanism of CE shows horizontal compression (e.g., Dziewonski and Woodhouse, 1983; Christensen and Ruff, 1985). By using a body-wave inversion method, Ward (1983) concluded that the depth of CE lies between 12 and 24 km, which is shallower than the depths of most compression type earthquakes listed in Chapple and Forsyth (1979). He suggested that the coupling at the subduction zone

* Present address: Institute of Geology, and Mineralogy, Faculty of Science, Hiroshima University, Hiroshima 730, Japan.

† Earthquake Research Institute, University of Tokyo, Tokyo 113, Japan.

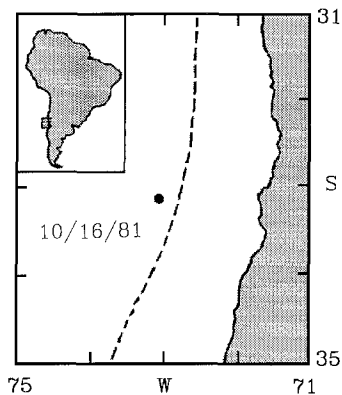


FIG. 1. The epicenter of October 1981 off Chile earthquake shown by black dot (Base map is after Christensen and Ruff, 1988).

may perturb the neutral plane of the bending stress. Christensen and Ruff (1983) found a spatial and temporal correlation between the occurrence of outer-rise earthquakes and large thrust type earthquakes and proposed a model in which the stress state of the subducting lithosphere at the outer-rise area may change before and after the occurrence of large thrust type earthquakes. Christensen and Ruff (1985) determined the depth of CE by single-station deconvolution technique and estimated its source depth ranging from 5 to 25 km. (This is depth below sea surface; in the following discussions, we use the "depth" as the one measured from sea surface, unless otherwise stated.) Their solution implies that the stress of the entire lithosphere may be in compression. The Harvard Centroid Moment Tensor solution gives 40 km as the centroid depth of CE, though this depth estimate may not be accurate enough considering the period of data used (>45 sec) in the inversions (Dziewonski and Woodhouse, 1983; see Discussion section also).

In the past 15 years, many authors have developed techniques to determine the source depth of shallow earthquakes accurately by using waveform modeling. Nábělek (1984) developed a body-wave inversion method which can determine simultaneously earthquake mechanism, source-time function, and source depth. Recently, two of the present authors (Seno and Honda, 1988; Honda and Seno, 1989) have developed new methods to determine source depths of shallow earthquakes. These two methods (described later) use the same technique to generate the waveforms, though there are differences in data sets and methods of analyses. Comparative studies of results obtained by a variety of methods are very few despite their importance. In this paper, we applied their methods (Seno and Honda, 1988; Honda and Seno, 1989) and Nábělek's to CE and compare the results. Part of the present results (the section of Simultaneous Inversion of Body- and Surface-Wave Data (IBS)) are also described in Honda and Seno (1989). In this paper, we will supplement their results. We find good agreement among the results of these three inversion methods, and the results suggest that the source depth of CE is around 20 to 45 km. This does not necessarily require the compression over the entire lithosphere as suggested by the previous workers.

SIMULTANEOUS INVERSION OF BODY- AND SURFACE-WAVE DATA (IBS)

Honda and Seno (1989) developed a moment-tensor inversion method which incorporates both body- and surface-wave data (hereafter IBS). Since it is necessary to explain the method to understand the results presented here, a brief description

of the method will be given below. The detail of the actual procedure can be found in Honda and Seno (1989).

Suppose we obtain a set of body-wave data at s stations, $y_1(t), \dots, y_i(t), \dots, y_s(t)$, (t : time) and a set of surface wave data at s' stations $p_1(\omega), \dots, p_j(\omega), \dots, p_{s'}(\omega)$ (ω : frequency). We try to find the components of moment tensor M_k ($k = 1, \dots, 6$) which minimize the residual

$$\delta = (1 - \lambda) \frac{1}{s} \sum_i \int_T \frac{(y_i(t) - \alpha_i Y_i(t))^2}{\sigma_i^2} dt + \lambda \sum_j \frac{(p_j(\omega) - P_j(\omega))^2}{\sigma^2}, \quad (1)$$

where

$$\sigma_i^2 = \int_T y_i(t)^2 dt \quad (2a)$$

$$\sigma^2 = \sum_j p_j(\omega)^2. \quad (2b)$$

$Y_i(t)$ and $P_j(\omega)$ are the synthetics of body waveform and surface-wave spectrum calculated for the assumed moment tensor M_k , source-time function and source depth. T is the length of the time window measured from the onset of a body wave (40 or 60 sec). λ determines the weight between the surface- and body-wave data and is set to 0.5 in this study (see Honda and Seno, 1989, for discussions). α_i is the amplitude correction term of each station for body waves and may include the effects of local structural variation beneath each station. The inversion is linear for a fixed coordinate of source, assumed α_i , and assumed source-time function. However, since we have to determine the appropriate starting position of the time window and the value of α_i for body-wave data, which are not known *a priori*, we iterate the procedures until the convergence of the solutions (i.e., M_k) is obtained. The depth and the shape of source-time functions are given as the parameters for the inversion. α_i is initially assigned as 1, then it will be changed systematically in each iteration (see Honda and Seno, 1989, for detail). A point source with no isotropic component is assumed. We define three types of residuals below:

surface wave, as

$$\delta_S = \sum_j (p_j(\omega) - P_j(\omega))^2 / \sigma^2 * 100, \quad (3a)$$

body wave, as

$$\delta_B = \frac{1}{s} \sum_i \int_T (y_i(t) - \alpha_i Y_i(t))^2 / \sigma_i^2 dt * 100, \quad (3b)$$

and combined, as

$$\delta_M = (\delta_S + \delta_B) / 2. \quad (3c)$$

These residuals are used to measure the fitness of the solutions and to infer the optimum depth and the source-time function. The synthetics of body waves are constructed based on the ray theoretical approach developed by Kroeger and Geller

(1983). For the crustal structure near the source region, we used the flat layer model tabulated in Table 1, which is the typical oceanic crustal structure. The water depth is measured in the bathymetric map at the epicenter. This structure is applied for the rest of methods. The attenuation parameter t^* for P waves is set to 1.0 sec (Futterman, 1962; Carpenter, 1966). We followed Kanamori and Given (1981) for the analysis of surface-wave data. They are analyzed at the single period of 256 sec.

The long-period vertical components of P waves from WWSSN and GDSN data are used as the body-wave data and IDA data are used for surface-wave data. This data set is the same as that of Honda and Seno (1989) and the detail of processing will be found in it (see Table 2 also).

TABLE 1
CRUST AND UPPER MANTLE STRUCTURE USED FOR
THE SOURCE AREA SHOWN FROM THE SURFACE

P -Wave velocity (km/sec)	S -Wave velocity (km/sec)	Density (g/cm ³)	Thickness (km)
1.5	0.0	1.03	4.5
2.0	1.0	1.90	1.0
4.7	2.70	2.40	1.6
6.6	3.82	2.80	4.5
8.1	4.65	3.35	infinity

TABLE 2
DATA USED IN EACH INVERSION METHOD

Network	Station			Methods		
	Name	Azimuth	Distance	IBS	Nábélek	Deconvolution
WWSSN	BLA	353.8	70.5	P	P	P
	BUL	113.1	88.4	P	P	
	LON	329.0	91.1			P
	MSO	335.0	90.4			P
	RAR	253.7	76.0	P	P	P
	WES	1.4	88.4	P	P	P
GDSN	ALQ	332.2	74.9	P	P, B, SH	
	AFI	253.7	89.5		P, B, SH	
	BOCO	358.5	37.8		SH	
	JAS	324.3	83.6	P	P, B, SH	
	LON	329.0	91.1		P, B, SH	
	SCP	356.3	74.1	P	P, B, SH	
	SNZO	224.5	82.9	P	P, B, SH	
IDA	CMO	333.4	113.6	2, 3		
	ERM	297.9	150.2	2, 3		
	ESK	34.0	106.5	2, 3		
	GUA	249.6	140.3	2, 3		
	KIP	290.7	97.4	2, 3		
	PFO	324.2	78.1	2, 3		
	RAR	253.7	76.0	2, 3		
	SPA	180.0	56.9	2, 3		
	SSB	45.5	105.1	2, 3		
	SUR	119.1	75.9	2		
	TWO	206.6	105.8	2, 3		

P : long-period vertical P waves; B : broadband P waves; SH : long period SH waves; 2, 3: R2 and R3 surface waves; Azimuth: measured at the epicenter from north (positive clockwise, in degrees); Distance: in degrees.

RESULTS OBTAINED BY IBS

It is well known that there exists a trade-off between the source depth and the duration of source-time function. A shallower depth estimation will be obtained as we assume broader source-time function. Since the source-time function is given *a priori* in IBS, we try several different types of source-time function with a variable time length. They are the isosceles triangular, rectangular, and two types of right-angled triangle. Honda and Seno (1989) only studied the triangular case. The way to choose the shape of source-time function is essentially infinite. The reason why we choose the simple source-time function described above comes from a rather *a posteriori* basis. As we shall see later, for the wide range of reasonable solutions, the shape of source-time function is almost an isosceles triangle. However, to check a possible trade-off between the other type of source-time function and the depth, we also use the rectangle and two types of right-angled triangles.

We show the distribution of residuals δ_B (body wave) of each case in Figures 2. The isocontours are drawn against the assumed depths (ordinates) and the half-time length of source-time function (abscissas). They are drawn for the values of $(\delta - \delta_{\text{minimum}})$. The plus marks in the figures indicate the positions where the calculations are done, and the asterisk shows the point where the residuals become the minimum.

We find that the residual of surface wave (δ_S) alone cannot constrain the depth, since there is no definite minimum in the residual δ_S . The residual of combined

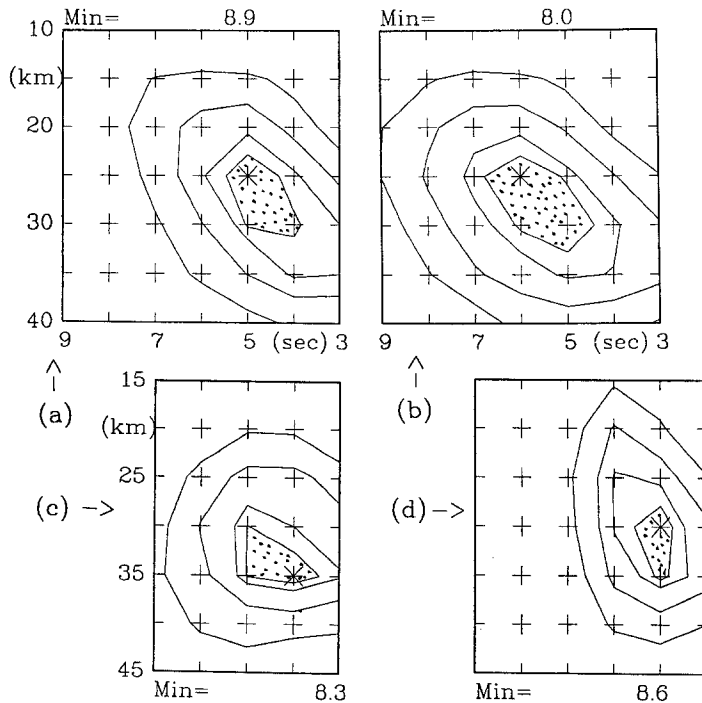


FIG. 2. The maps show the residual distribution δ_B against the depths (ordinate) and half widths of source-time functions (abscissa). The contours are drawn for the values $(\delta - \delta_{\text{minimum}})$ at 0.5, 1., 2.5, and 5. The minimum values (δ_{minimum}) are shown in numerals at either the top or bottom of each figure. The dotted area is used for the estimation of depth (see text). (a) The source-time function is a right angled triangle. The apex is situated at the start. (b) The source-time function is an isosceles triangle. (c) The source-time function is a right angled triangle. The apex is situated at the end. (d) The source-time function is a rectangle.

data δ_C only reflects δ_B , since the variation of δ_S (<0.5) is much smaller than that of δ_B . Therefore, we do not take into account the residual of both δ_S and δ_C for the estimation of the optimum depth and source-time function. It was shown that the surface-wave data of a single period alone cannot constrain the source depth (Romanowicz, 1981). However, it is necessary to include the surface-wave data in IBS to stabilize the solution (Honda and Seno, 1989). Also, we note here that such a "flat" distribution of δ_S can be obtained only if the amplitude term α_i is included. If α_i is fixed, an apparent variation of δ_S appears because of the constraint by the amplitude of body-wave data. The magnitude of moment tensors is constrained by both surface- and body-wave data. If we use only long-period surface-wave data, the moment increases as the assumed source depth becomes deeper. On the contrary, if only the body-wave data are used, it increases as the assumed source depth becomes shallower or the length of source-time function becomes longer. This may, at a first look, suggest that there is an optimal solution which satisfies the amplitudes of both surface- and body-wave data. However, since the body-wave data are more susceptible to the local structure than the long-period surface-wave data are, it is desirable to suppress the body-wave data in determining the magnitude of moment tensor. The present method has such a character by the inclusion of α_i , and it has been confirmed. In IBS, the magnitude of moment tensor and the depth are respectively constrained by the surface-wave data and body-wave data (Honda and Seno, 1989).

We infer the optimum depth by varying the depths and taking the depth where the residuals become minimum for each type of source-time function. It is from 25 to 35 km. The dotted area in Figure 2 shows where the deviation of δ_B is within 0.5 from the minimum values. Since the variation of δ_S (i.e., surface-wave data) is less than 0.5 for almost whole parameter ranges we studied, this area may correspond to the uncertainty of each solution. Taking account of this uncertainty, we estimate the centroid depth of CE is from 20 to 35 km. Considering the simpleness of source-time functions as shown in the later analyses, we believe that this estimate (20 to 35 km) is not overly biased by the selection of the shape of source-time function. However, it is necessary to determine the depth in more self-consistent way, say, by combining the present method with the deconvolution approach. The final moment-tensor solution obtained in this method is described in Tables 3a through d (isosceles triangular source-time function with 25 km depth). We also show the obtained α_i for this solution in Table 3d. This solution is the same as that of Honda and Seno (1989) and the fit of the final solution to the data will be found in it.

NÁBĚLEK'S BODY-WAVE INVERSION METHOD

Nábělek (1984) developed the body-wave inversion method which can determine the mechanism, source depth, and source-time function, simultaneously. Teleseismic Green's functions for both P and SH waves are calculated using Haskell matrices, in which the effect of layered velocity structures for both source and receiver can be included. The maximum likelihood inverse of synthetic and observed seismograms are then performed to obtain model parameters, using a standard iterative least-squares inversion technique. The parameters for which we try to solve in this paper are a double-couple source mechanism, a scalar moment, a source-time function, and a centroid depth. The source-time function is parameterized by overlapping isosceles triangles (length = 2 sec), and we impose a positivity constraint in the present paper. For the Futterman's parameter t^* (Futterman, 1962), we use

TABLE 3a
SOURCE COORDINATES AND ORIGIN TIME REPORTED BY ISC

Origin Time	Epicenter	Focal Depth	Magnitudes	
			M_b	M_s
16 Oct. 1981 03h 25m 40s	33.15S 73.10W	18 km	6.2	7.2

TABLE 3b
MOMENT-TENSOR SOLUTIONS

	Mrr	Mtt	Mff	Mrt	Mrf	Mtf
IBS	6.11 (0.97)	-0.20 (-0.03)	-5.90 (-0.94)	-0.38 (-0.06)	1.43 (0.23)	-1.42 (-0.23)
Nábělek	9.20 (0.99)	-0.32 (-0.03)	-8.88 (-0.96)	-0.53 (-0.06)	-0.87 (-0.09)	-1.72 (-0.19)

Unit: 10^{26} dyne·cm (see Dziewonski and Woodhouse, 1983, for notation). The values in the parenthesis show the normalized moment tensor. The normalization constant M_0 is shown below.

TABLE 3c
BEST DOUBLE COUPLE* AND DOUBLE COUPLE SOLUTIONS

	M_0	Strike (°)	Dip (°)	Slip (°)	Depth (km)
IBS	6.35×10^{26} dyne·cm	199.7	39.4	99.9	25
Nábělek	9.26×10^{26} dyne·cm	193.1	48.0	92.9	27.7

* Dziewonski and Woodhouse, 1983.

TABLE 3d
SCALING FACTORS (α)

Station	α
JAS*	0.70
SNZO*	1.09
BUL	1.16
WES	0.83
BLA	0.62
RAR	0.55
ALQ*	1.03
SCP*	0.81

*Implies GDSN station.

1.0 and 4.0 sec for P and S waves, respectively. The detail of this method is given in Nábělek (1984).

The data we used are taken from long-period components of GDSN and WWSSN data. GDSN P waves and SH waves are processed for the analysis. We also calculate the broadband P wave from several stations (SCP, ALQ, LON, JAS, AFI, and SNZO), following Harvey and Choy (1982). The filter used for the broadband data has a flat response from 15 mHz to 1.8 Hz. The data preparation for WWSSN P -wave data is the same as described in the section entitled IBS. The data of P and SH waves are shown in Figures 3a and 3b, respectively. A brief description of data set is described in Table 2.

RESULTS OBTAINED BY NÁBĚLEK'S METHOD

We give the final mechanism solution and source-time function in Figures 3 (see Table 3 also) along with the fit of synthetics to the data. The depth is 27.7 km and the obtained standard deviation is ± 0.4 km. However, since the inversion is nonlinear, this value may be only nominal. Nábělek (1984) suggested that 10 times the standard deviation is the appropriate uncertainty. There may be about ± 5 km of error associated with the depth estimate.

We check the residuals carefully by the deconvolution in which the focal mechanism is fixed to the final solution. For the different sets of data (broadband, WWSSN, and GDSN long-period data), the depth is varied and source-time function is deconvolved. The results are shown in Figures 4. The residuals shown in these figures are normalized by the power of the data, and are the same as described in the section entitled IBS. Generally, the scalar moment decreases as the depth increases. This occurs because the time difference between the direct phase and reflected waves (i.e., pP , sP , pwP ...) is short at the shallow depth. They will interfere destructively, hence the scalar moment amplitude becomes large to com-

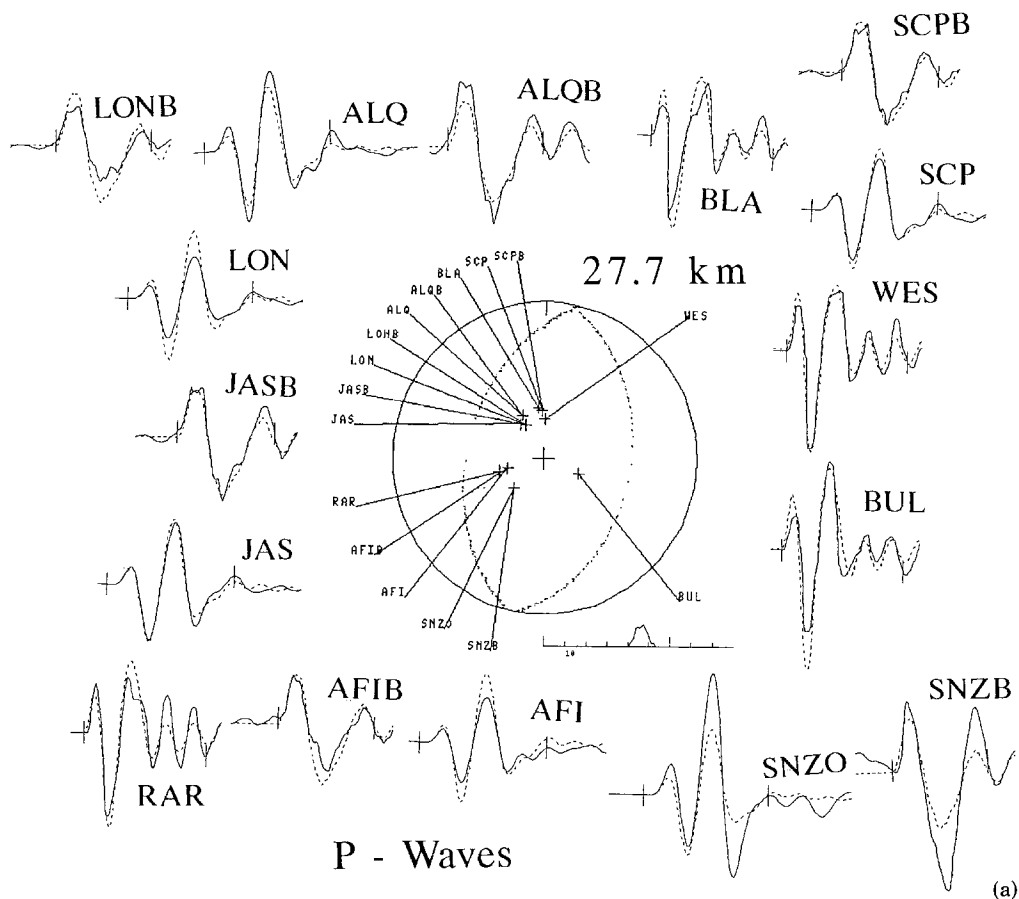
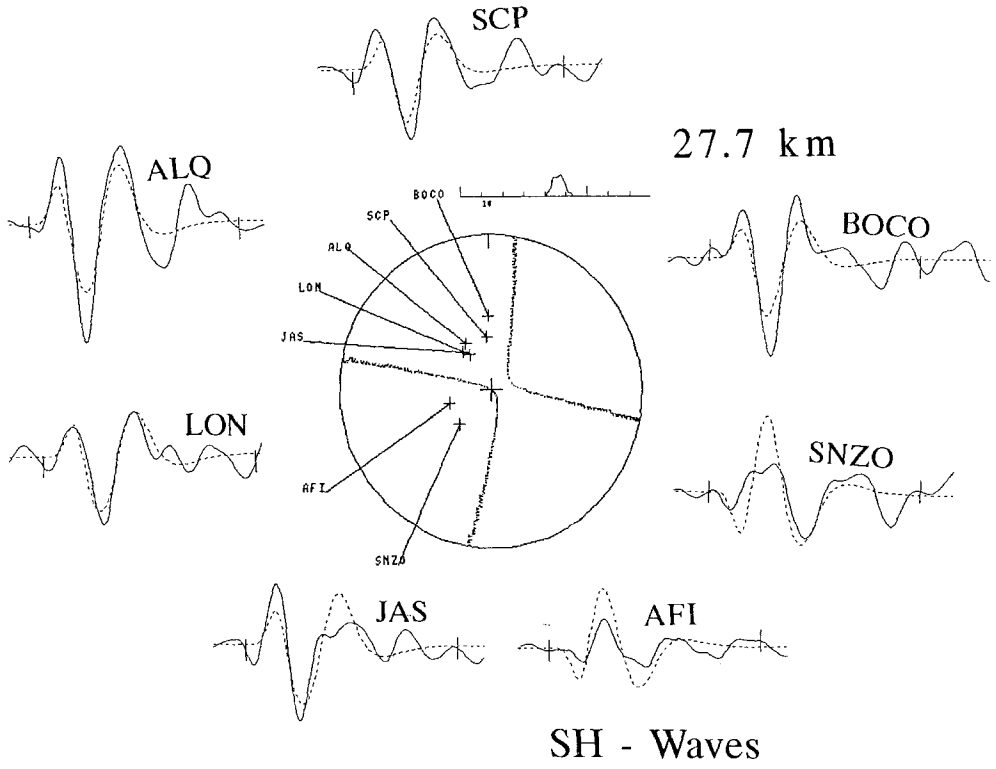
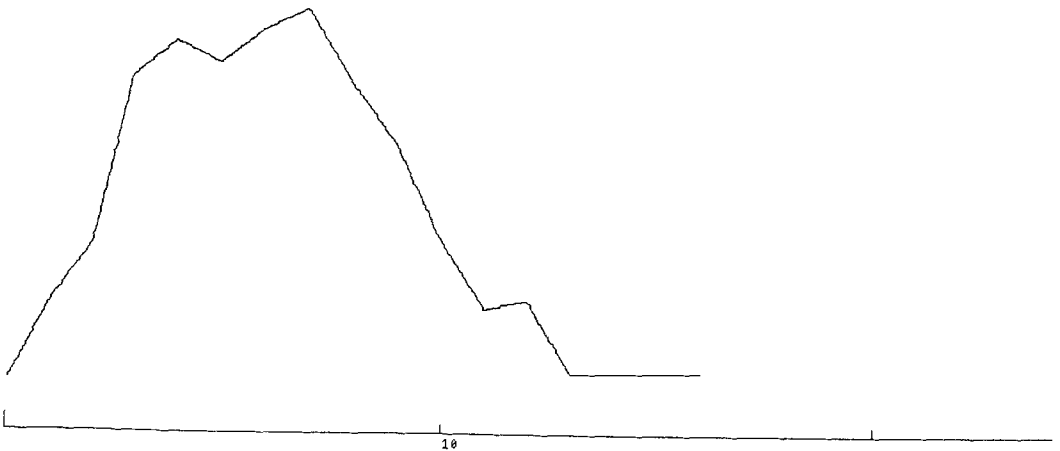


FIG. 3. The solution obtained by Nábělek's method. Fit of data to synthetics (shown by dotted lines) is also shown. (a) Mechanism solution (shown in dotted lines) and P waves. The letter 'B' attached to the station names indicates the broadband data. A small inset shows the source time function. (Tick interval is 10 sec which is also applicable for other seismograms.) (b) Radiation pattern of SH waves (shown in dotted lines). Long-period data are used. (c) Close up of obtained source-time function. Tick interval is 10 sec.



(b)



(c)

FIG. 3. (Continued).

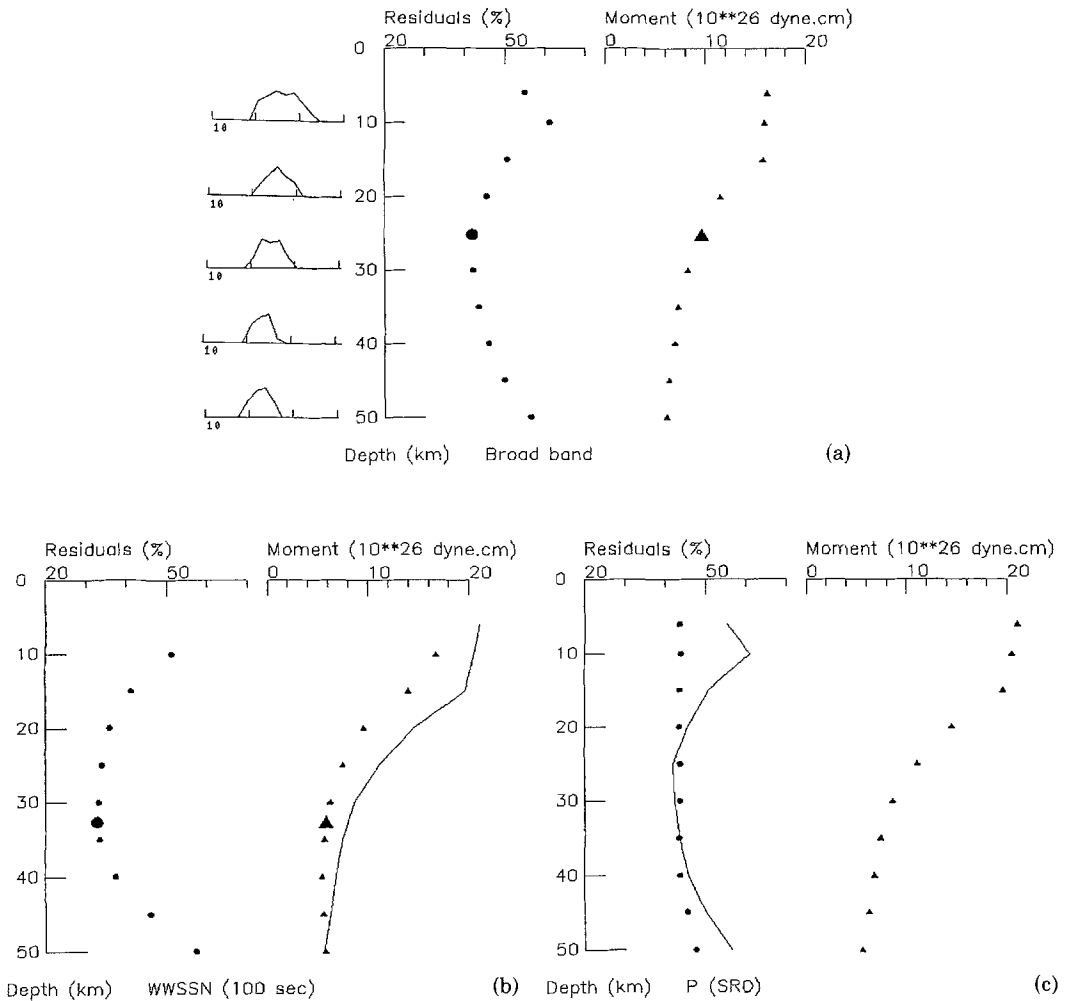


FIG. 4. The residuals and scalar moments determined by the deconvolution. (a) Deconvolved results for the broadband data. The diagrams attached to the left show the obtained source-time functions. The tick interval is 10 sec. The larger filled circles and triangles show the position where the residuals become minimum. (b) Deconvolved results for WWSSN data. The line shown in the scalar moment diagram is obtained by the deconvolution of GDSN data alone (see (c) also). Note that the scalar moments obtained for WWSSN data are systematically smaller than those for GDSN data. The other notations are the same as those described in (a). (c) Deconvolved results for long-period GDSN data. The line in the residuals is obtained by the deconvolution of WWSSN data alone (see (b) also). There is no depth resolution in this data set.

penetrate the destructive interference. Broadband data and WWSSN data set give a fairly good constraint in the sense that there exists a minimum in the residuals (see Figs. 4a and 4b), while GDSN long-period data (*P* waves) cannot constrain the depth (Fig. 4c). Note that the shape of source-time function of the final solution (depth = 27.7 km) is triangular whose width is about 12 sec (Fig. 3c). This is consistent with the best solution discussed in the previous section (triangular source-time function at 25 km: Fig. 2a).

We note here that the scalar moments obtained by GDSN long-period data is systematically greater than those by WWSSN data (Fig. 4b). In IBS, it was also found that the average of the station correction terms α_i (described in the section

entitled IBS; in Nábělek's inversion, we do not take into account the amplitude correction term) for GDSN stations is more than 10 per cent higher than that for WWSSN stations (see Table 3).

Figures 4a and 4b respectively give the depths of the minimum residual to be around 25 km to 33 km for the broadband and the WWSSN data sets. The difference in the depth estimates may partly come from the different frequency content and from the different station coverage of the two data sets. We also suggest that the difference may be intrinsic of the problem. For an earthquake of this size, a point source representation of its rupture, using first-motion body waves, may not be meaningful. (We consider this in the next section.) Although the minimum residual depths in Figure 4a (broadband) and 4b (WWSSN) are different, the depth ranges where residuals are within 5 per cent of the minimum residuals are almost the same, and they are between 20 km and 40 km. We thus infer that the centroid depth of CE is located somewhere between a depth of 20 km and 40 km, which may also be the location of the distributed sources. Comparing with Figures 2 and the discussion in the IBS section, this error estimate is probably a safe one. The residuals shown in Figure 4 are much larger than those in Figures 2, where residuals are about 10 ~ 15 per cent. This is because in Nábělek's method we fit the absolute size of waveforms while in IBS some of the misfits are absorbed in the coefficients α_i .

DECONVOLUTION OF BODY WAVES BY ASSUMING THE DISTRIBUTED POINT SOURCES

Deconvolution of seismograms has been used to determine source depth (Forsyth, 1982; Christensen and Ruff, 1985). Christensen and Ruff (1985) showed that deconvolution assuming an incorrect source depth usually leads to a complex source-time function. They assumed that the depth range, where the deconvolved source-time function is simple, is the optimum depth range. They also showed that the fit to the data by the synthetics calculated from the deconvolved source-time function is almost the same at any assumed depth. This occurs partly because their time span of the deconvolution is as long as the data time window, resulting in the solutions which fit data equally well at any depth. Also, in their deconvolution, they assumed a point source. Several workers (e.g., Stein and Wiens, 1986) showed that the point source approximation often fails to give a correct depth for larger ($M_s \sim 7.0$) earthquakes. Seno and Honda (1988) deconvolved the long period P waves by assuming vertically distributed point sources in order to determine the source depths of shallow earthquakes. Since we use their method to analyze the centroid depth of CE in this section, we describe their method briefly below.

Point sources are vertically distributed with an equal grid space. The rupture starts at either the top or bottom of the distributed source, and propagates downward or upward. A rupture velocity of 3 km/sec is assumed. The method to calculate the Green's functions are the same as that described in the IBS section. The source-time function is parameterized by overlapping isosceles triangles (length 3 sec). The source mechanism used is the best double couple solution determined by IBS (Table 3). The depths of the starting and ending points of the rupture are changed to find minimum residuals. The residuals are defined by

$$\text{res.} = \int_T (x_{\text{obs}}(t) - x_{\text{syn}}(t))^2 dt / \int_T (x_{\text{obs}}(t))^2 dt * 1000, \quad (4)$$

where x_{obs} is the observed seismogram, x_{syn} is the synthetic seismogram, and T is the time window of the data. The data are taken from WWSSN long-period vertical P waves (Table 2). They are digitized and linearly interpolated; a sampling rate of 1 sec is used for the data.

We first deconvolve the data with the same time span of a source-time function as that of data using a damped least squares (Ruff and Kanamori, 1983). From this inversion we can find a source duration for a point source assumed at each depth. Noting that the source duration for a point source should be longer than that of vertically distributed sources (i.e., we assume that a rupture propagates mainly in the vertical direction), we may estimate a maximum source duration from this procedure. Then we perform a deconvolution with a shorter time span of the source-time function than that of the data but longer than the maximum duration for the point sources. We regard the depth extent which gives the minimum residuals as the optimum depth extent. Details of this method will be described in a separate paper (Seno and Honda, manuscript in preparation).

RESULTS OBTAINED BY DECONVOLUTION

In Figure 5, we show an example of deconvolved source-time function at WES when we use the time span of the deconvolution as long as that of data and a 10 km grid distance. The residuals (i.e., equation 4) are shown by numerals below each source-time function. The numerals in the abscissa indicate the starting depth and those of the ordinate indicate the final depth of rupture (km). The source-time functions from 20 to 40 km point source depth look "simple" and give smaller residuals than the other point source solutions. Similarly there are the solutions with finite depth extents which give small residuals or simple source-time functions (e.g., 20–30; we use the notation XX–YY for a solution with a finite depth extent which implies that a rupture starts at XX km and stops at YY km). In this long time span deconvolution, we cannot take the depth which gives the minimum residuals as the optimum depth because the time length of source-time function is

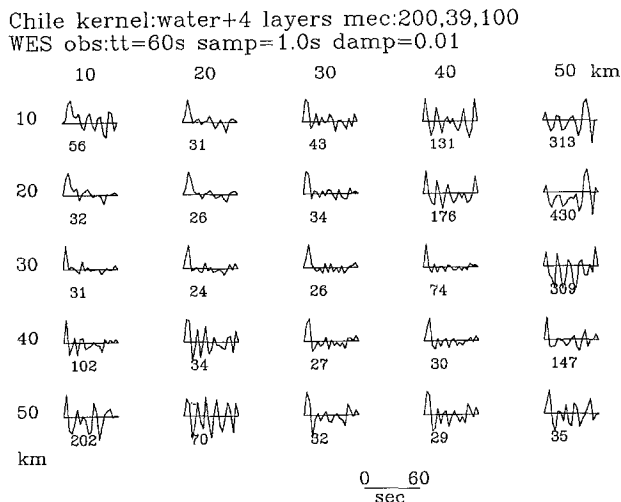


FIG. 5. Source-time functions obtained by the deconvolution using distributed sources. The time span of the deconvolution is 60 sec which is the same as that of data. The abscissa and ordinate show the starting and ending depth of rupture (km). Numerals show the residuals (see equation 4). The numerals shown in the side of 'mec' in the header indicate the focal mechanism used (i.e., strike, dip, and slip in degrees). Only station WES is shown.

so long that the source-time function can be adjusted to fit the data equally for a wide range of assumed depth, as discussed by Christensen and Ruff (1985). (Note the residuals of 20–20 and 30–30.) Furthermore, we found that the simplicity criterion advocated by Christensen and Ruff (1985) is not effective; the solution 40–30 gives a simple source-time function, though it gives large residuals. Therefore, we proceed to the next step in which we constrain the time span of the source-time function. From the deconvolved source-time functions for the point sources from 20 to 40 km, we infer that the source duration is less than 15 sec. The results of deconvolution do not depend seriously on the length of source-time function used in the inversion, unless it is so long that the inversion becomes unstable.

Figure 6 shows the deconvolved source-time functions for each station when we use 24 sec for the length of the deconvolution. Note that the residuals shown in Figure 6 are subtracted from the minimum residuals shown below each figure. The results show that CE is represented by a point source whose depth is 30 or 40 km except for station RAR. The shape of the source-time function at the optimum depth are triangular and their width is about 10 sec, if we neglect the later undulations after the main pulse. This is consistent with the results described in the previous two sections.

RAR shows the minimum residuals at 20–10. However, there is a local minimum residual at 30 km point source depth and this gives a simpler source-time function. If we deconvolve the source-time function using a 5 km grid for this station, the minimum residual is located at 35–30. Thus the minimum residual for the 10 km grid at 20–10 is the artifact caused by the usage of the coarse grid. Using a 5 km grid space for the other stations gives the following results: BLA: 45–40, LON: 40–35, MSO: 45–35, and WES: 30–35. Thus they are consistent with the results for the 10 km grid space, that is, the depth extent of CE is around 10 km and the centroid depth is located somewhere between 25 and 45 km.

DISCUSSION

We have summarized our results and those of other studies in Figure 7. Our results show a good consistency among them (IBS, N: Nábělek's method and D: Deconvolution method), which suggests that the depth of CE is between 20 and 45 km. We have confirmed the centroid depth of Harvard CMT solution (HVD) to be about 40 km, by performing a similar inversion using a program written locally (Kawakatsu, 1989). We compared the residuals of the CMT solutions with fixed depths as we did in Figures 4. The residual minimum is located around a depth of 40 km, but the changes of the residual for different source depths are small. Only 2 per cent change of residuals (the minimum residual is 59.6 per cent) is obtained for the depth variation from 25 to 60 km. However, considering that the solution is obtained from a long-period data set (>45 sec), we should prefer the depth estimates obtained by other methods.

Our results are in contrast with those obtained by Christensen and Ruff (1985) (CR) and Ward (1983) (W) which suggest the shallow source (less than 25 km). Ward (1983) used only long-period GDSN data including diffracted *P* and *S* waves. However, as we show, using GDSN data alone cannot constrain the source depth well (see Fig. 4c). Actually, the residual distribution shown by Ward (1983) has only broad minimum, and its tendency is very similar to our result; i.e., the residuals decrease monotonically as the assumed depth decreases. Thus, we think that there is no resolution in long-period GDSN data to determine the source depth for this earthquake.

Christensen and Ruff (1985) used the simplicity criterion of source-time function deconvolved by P waves to find the optimum depth extent; i.e., they considered the point source depths which give simple source-time functions as the rupture extent. However, it would not be straightforward to conclude that the rupture extent is over the depths which give a simple source-time function, because the Green's function generated from a finite rupture is different from that of a point source. For example, in Figure 5, we can see that the source-time function is simple for the point sources from 20 to 40 km. However, the rupture from 20 to 40 km (20–40) or that from 40 to 20 km (40–20) gives a very complicated source-time function (Fig. 5). This indicates that we need to calculate Green's functions from finite sources if we want to retrieve the depth extent.

As we noted earlier, using only the simplicity criterion of Christensen and Ruff (1985) is not reasonable; the 40–30 solution of Figure 5 gives a simple source but

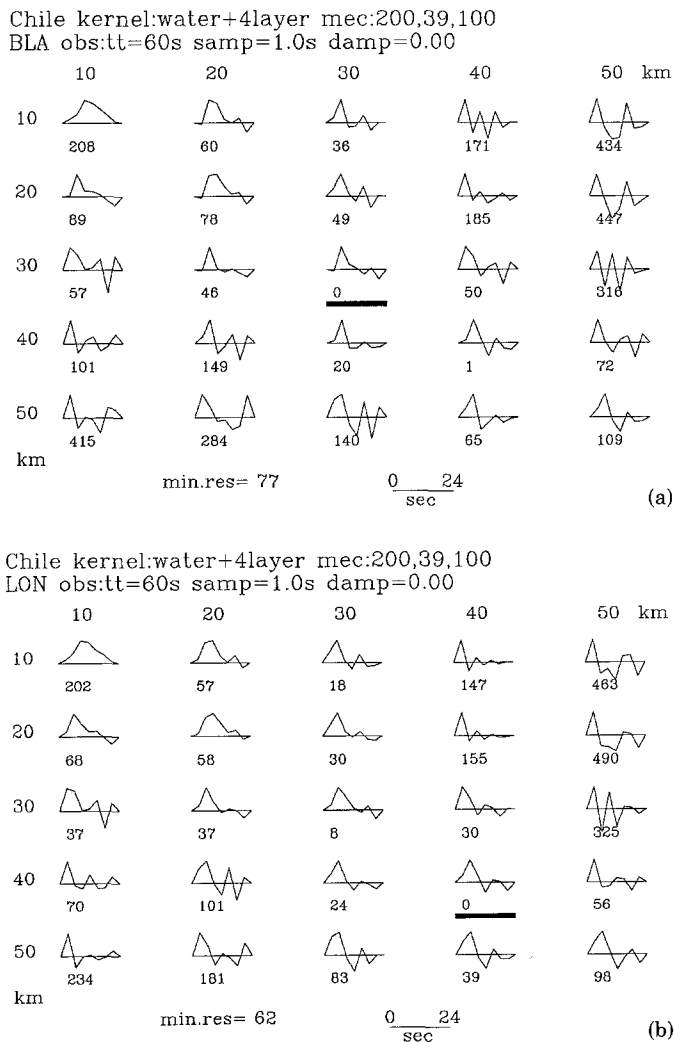
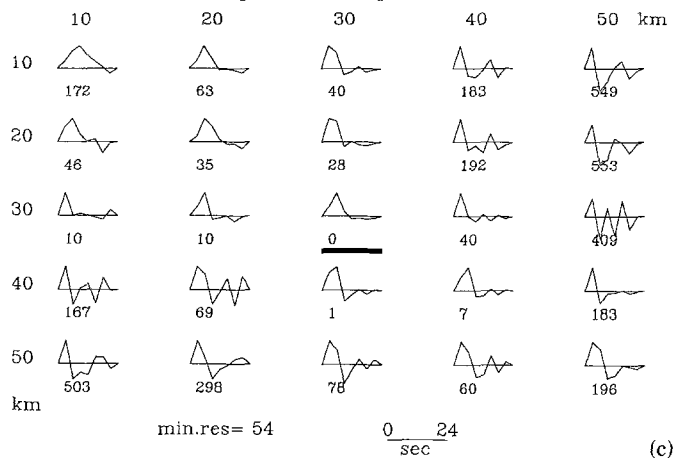
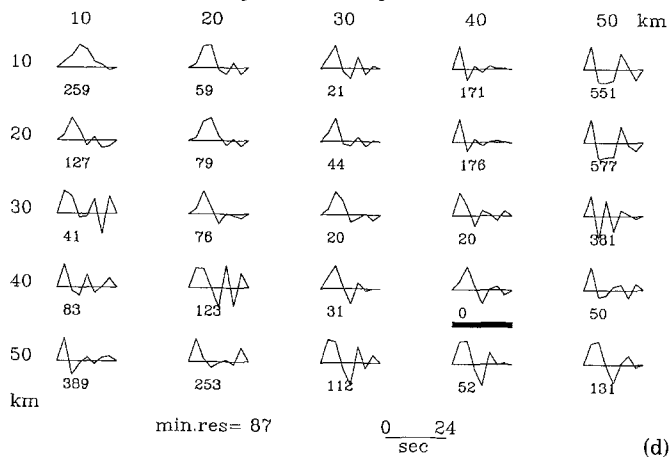


FIG. 6. Same as Figure 5. The time span of the deconvolution is 24 sec which is smaller than data length (60 sec). Bold lines show the position where the residual becomes minimum. Residuals are subtracted from the minimum values which are shown below each figure. (a) Station BLA. (b) Station LON. (c) Station WES. (d) Station MSO. (e) Station RAR.

Chile kernel:water+4layer mec:200,39,100
 WES obs:tt=60s samp=1.0s damp=0.00



Chile kernel:water+4layer mec:200,39,100
 MSO obs:tt=60s samp=1.0s damp=0.00



Chile kernel:water+4layer mec:200,39,100
 RAR obs:tt=60s samp=1.0s damp=0.00

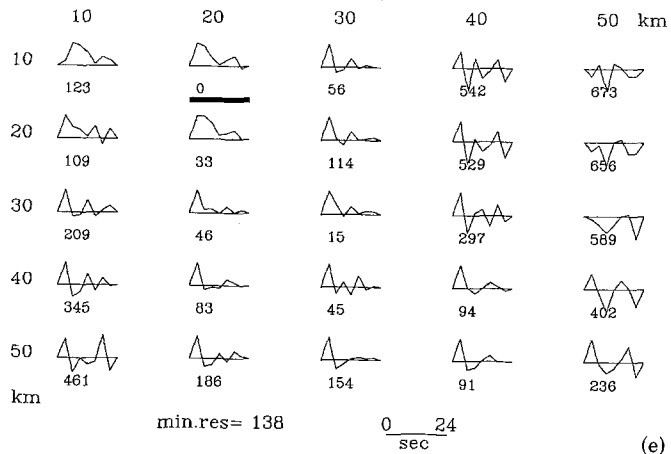


FIG. 6. (Continued).

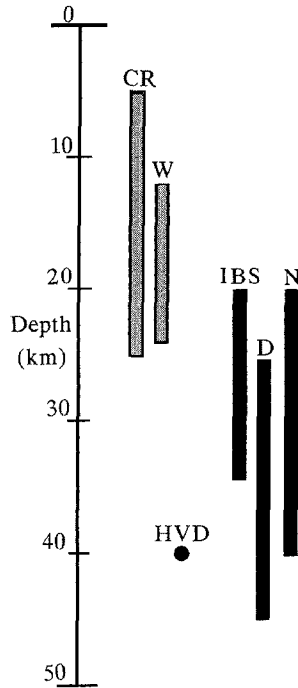
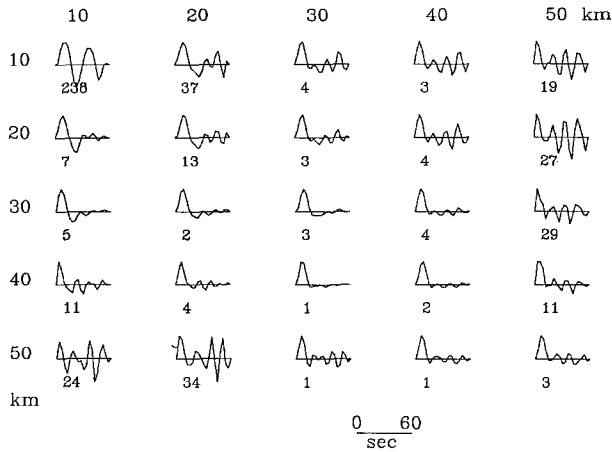


FIG. 7. Summary of present results and previous results. CR: Christensen and Ruff (1985); W: Ward (1983); HVD Harvard Centroid Moment Tensor solution (Dziewonski and Woodhouse, 1983). IBS: Inversion of Body and Surface waves; D: Deconvolution method; N: Nábělek's (1984) method.

very large residuals. Probably we have to take into account both the simplicity and residuals. In this study and Seno and Honda (1988), we restrict the time span of the source-time function shorter than the data time window and take into account only the minimum residuals in determining the depth. Such a restriction of the source-time function prohibits the later part of the source-time function to adjust to fit the later phase of the data, thus it is equivalent to pose a kind of simplicity on the source-time function. This argument also applies for IBS in which we use simple and restricted source-time functions.

Another defect of the method of Christensen and Ruff (1985) arises from the fact that they used a simple crustal structure; a water layer + half-space. Seno and Honda (1988) examined the effect of this by generating the synthetics 27–42 (i.e., a rupture starts at 27 km and stops at 42 km) calculated on the structure described in Table 1. Then, they deconvolved the synthetics using either the same crustal structure as given in Table 1 (Fig. 8a) or the simple water + half-layer model (Fig. 8b). When we use the simple crustal structure, we can find simple sources for the point sources of which depth lies between 10 and 40 km (Fig. 8b). In contrast, when we use the same crustal structure as in the synthetics, we can obtain simple source-time functions only around 30 and 40 km point source depths, which are within the rupture extent used in the synthetics. This indicates that if we use a simpler crustal structure than the real one, an incorrect depth extent may be obtained from the simplicity criterion proposed by Christensen and Ruff (1985). The reason why the shallow depth as 10 km resulted in a simple source-time function when we use a simple crustal structure is not obvious, because the shape of Green's function varies in a complicated way with depth. However, it is shown that the shape of the source-time function strongly depends on the assumed crustal

(a) Chile kernel:water+4 layers mec:205,45,120
 WES synth:h=27-42(3)km water+4 layers damp=0.01



(b) Chile kernel:water+half space mec:205,45,120
 WES synth:h=27-42(3)km water+4 layers damp=0.01

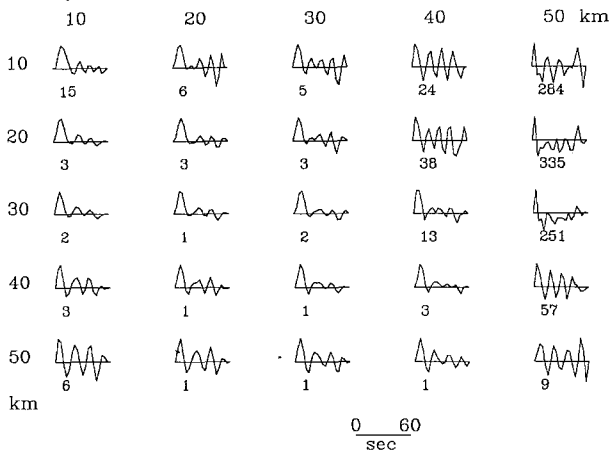


FIG. 8. Same as Figure 5. These are taken after Seno and Honda (1988). The synthetics are constructed for the focal mechanism shown in this figure (i.e., strike = 205°; dip = 45°; slip = 120°), and the crustal structure given in Table 1. (a) The structure used for the deconvolution is the same as described in Table 1. (b) The structure used for the deconvolution is water + half space.

structure. On the contrary, the residuals of both cases (Figs. 7a and 7b) show much more reasonable behavior.

Seno and Honda (1988) compiled the depth distribution of smaller outer-rise earthquakes versus the age of plate at the trench. They found the general tendency that the earthquakes of compression type are deeper than those of extension type. The compressional events are distributed from 20 to 40 km at 30–40 Ma, which is the age of subducting Nazca plate where CE occurred. Thus the centroid depth and depth extent of CE are consistent with the distribution of the smaller compressional events. This suggests that CE is likely to be caused by the compressional bending stress within the Nazca plate prior to its subduction. A stress perturbation due to seismic coupling, if any, is not so large as inferred by Ward (1983) and Christensen and Ruff (1988). However, we do not deny a possibility that the compression type outer-rise earthquakes may be triggered by the stress concentration before the

occurrence of major thrust zone earthquakes (Christensen and Ruff, 1983; Astiz and Kanamori, 1986; Dmowska et al, 1988; Lay et al, 1989). More detailed analysis of the stress perturbation is described in a separate paper.

CONCLUSIONS

We studied the depth of October 1981 outer-rise earthquake off Chilean coast using three different waveform inversion methods. Their results show good agreement with each other, which suggests that the centroid depth of this event is located between 20 and 45 km and its rupture extent is around 10 km.

We found that GDSN long-period data alone cannot constrain the depth for this earthquake. The shape of deconvolved source-time function is strongly dependent on the assumed sources (i.e., point source or distributed sources) and the crustal structure. Thus, it is not appropriate to use it as the criterion for determining the depth.

The above results suggest that the Chile earthquake occurred due to the compressional stress associated with the bending of the subducting oceanic lithosphere.

ACKNOWLEDGMENTS

We thank Drs. Thorne Lay and David M. Boore for their thorough reviews and suggestions to improve the manuscript. Dave Yuen kindly provided us the computer facility for preparing manuscripts. Kris Lund helped us in preparing figures. We thank both of them. S.H. is the recipient of a visiting research fellowship from the Minnesota Supercomputer Institute, University of Minnesota. A part of the calculation was done using Cray X-MP/216 at Research Information Processing System, Agency of Industrial Science and Technology, Japanese Government.

REFERENCES

- Astiz, L. and H. Kanamori (1986). Interplate coupling and temporal variation of mechanisms of intermediate-depth earthquakes in Chile, *Bull. Seism. Soc. Am.* **76**, 1614–1622.
- Carpenter, E. W. (1966). Absorption of elastic waves: an operator for constant Q mechanism, Rep. 0-41366, At. Weapons Res. Estab., London.
- Chapple, W. M. and D. W. Forsyth (1979). Earthquakes and bending of plates at trenches, *J. Geophys. Res.* **84**, 6729–6749.
- Christensen, D. H. and L. J. Ruff (1983). Outer-rise earthquakes and seismic couplings, *Geophys. Res. Lett.* **10**, 697–700.
- Christensen, D. H. and L. J. Ruff (1985). Analysis of the trade-off between hypocentral depth and source time function, *Bull. Seism. Soc. Am.* **75**, 1637–1656.
- Christensen, D. H. and L. J. Ruff (1988). Seismic coupling and outer-rise earthquakes, *J. Geophys. Res.* **93**, 13421–13444.
- Dmowska, R., J. R. Rice, L. C. Lovinson, and D. Josell (1988). Stress transfer and seismic phenomena in coupled subduction zones during earthquake cycle, *J. Geophys. Res.* **93**, 7869–7884.
- Dziewonski, A. M. and J. H. Woodhouse (1983). An experiment in systematic study of global seismicity: centroid-moment tensor solutions for 201 moderate and large earthquakes of 1981, *J. Geophys. Res.* **88**, 3247–3271.
- Futterman, W. I. (1962). Dispersive body waves, *J. Geophys. Res.* **67**, 5279–5291.
- Harvey, D. and G. L. Choy (1982). Broadband deconvolution of GDSN data, *Geophys. J. Roy. Astr. Soc.* **69**, 659–668.
- Honda, S. and T. Seno (1989). Seismic moment tensors and source depths determined by the simultaneous inversion of body and surface waves, *Phys. Earth Planet. Interiors* (in press).
- Kanamori, H. and J. W. Given (1981). Use of long-period surface waves for fast determination of earthquake source parameters, *Phys. Earth Planet. Interiors* **27**, 8–31.
- Kawakatsu, H. (1989). Centroid single force inversion of seismic waves generated by landslides, *J. Geophys. Res.* **94**, 12363–12374.
- Kroeger, G. C. and R. J. Geller (1983). An efficient method for computing synthetic reflection seismograms for plane layered models, *EOS* **64**, 772.
- Lay, T., L. Astiz, H. Kanamori, and D. H. Christensen (1989). Temporal variation of large intraplate earthquakes in coupled subduction zones, *Phys. Earth Planet. Interiors* **54**, 258–312.

- Nábělek, J. L. (1984). Determination of earthquake source parameters from inversion of body waves, *Ph.D. Thesis*, Massachusetts Institute of Technology, Cambridge, Massachusetts.
- Romanowicz, B. (1981). Depth resolution of earthquakes in central Asia by moment tensor inversion of long period Rayleigh waves: effects of phase velocity variations across Eurasia and their calibration, *J. Geophys. Res.* **86**, 5963–5984.
- Ruff, L. and H. Kanamori (1983). The rupture process and asperity distribution of three great earthquakes from long-period diffracted *P*-waves, *Phys. Earth Planet. Interiors* **31**, 202–230.
- Seno, T. and S. Honda (1988). Depth extent of large trench-outer-rise earthquakes, *EOS* **69**, 1317.
- Stein, S. and D. A. Wiens (1986). Depth determination for shallow teleseismic earthquakes: method and results, *Rev. Geophys.* **24**, 806–832.
- Stauder, W. (1968). Tensional character of earthquake foci beneath the Aleutian trench with relation to sea floor spreading, *J. Geophys. Res.* **73**, 7693–7701.
- Ward, S. N. (1983). Body wave inversion: moment tensors and depths of oceanic intraplate bending earthquake, *J. Geophys. Res.* **88**, 9315–9330.

IISEE, BUILDING RESEARCH INSTITUTE
TSUKUBA, IBARAKI 305, JAPAN
(S.H., T.S.)

MINNESOTA SUPERCOMPUTER INSTITUTE
MINNEAPOLIS, MINNESOTA 55415
(S.H.)

GEOLOGICAL SURVEY OF JAPAN
TSUKUBA, IBARAKI 305, JAPAN
(H.K.)

DEPARTMENT OF GEOLOGY AND GEOPHYSICS
UNIVERSITY OF MINNESOTA
MINNEAPOLIS, MINNESOTA 55455
(S.H.)

Manuscript received 15 March 1989